an optimal value, which include the linear prediction (LP) filter model order and the truncation dimension. Complicated procedures have been proposed to choose these two parameters in the original publication, which rely on a simplified matrix perturbation model to determine the noise threshold and a separate LP analysis has to be performed to ascertain the noise variance. The reconstruction dimension for the MCP filter is determined using statistics obtained from a run-time SVD decomposition. This procedure does not depend on any particular assumption. The better performance as well as the robustness and easiness of its parameter determination are advantages of MCP as compared to DCT filter.

One novelty of the MCP filter is that it is motivated from treating the filtering problem as an empirical data-driven modeling of ECG and its associated parameter estimation. In this sense, the MCP filter serves as an example of deriving new forms of ECG subspace filters. From the results presented in the paper, the most important further development concerning MCP filter should probably be directed at improving the robustness of DTW of two noisy ECGs and exploring the distance between two aligned ECGs to handle the different morphological beats in MCP modeling. The necessity of the former effort is evident since the ideal MCP filter achieved comparable results as the GF and was more robust to the degree of heart rate variability. The later is also important since the occupance of abnormal beats in real ECG is not uncommon.

Finally, the present form of MCP filter only explores the temporal redundancy within a single lead ECG. It can be expanded to a multiple lead scenario without difficulty. Indeed, the modification of a MCP model to a multilead-multicycle (MLMC) one may be the key for the discovery of critical hidden dynamics in a noisy environment.

ACKNOWLEDGMENT

The authors would like to thank the anonymous reviewers and Dr. L. Iasemidis for their constructive comments which helped greatly improve the original manuscript.

REFERENCES

[1] O. Pahlm and L. Sornmo, "Data processing of exercise ECGs," *IEEE Trans. Biomed. Eng.*, vol. BME-34, no. 1, pp. 158–165, Jan. 1987.

[2] V. X. Afonso, W. J. Tompkins, T. Q. Mguyen, K. Michler, and L. Shen, "Comparing stress ECG enhancement algorithms," *IEEE Eng. Med. Biol. Mag.*, vol. 15, no. 3, pp. 37–44, May–Jun. 1996.

[3] N. Nikolaev, A. Gotchev, K. Egiazarian, and Z. Nikolov, "Suppression of electromyogram interference on the electrocardiogram by transform domain denoising," *Med. Biol. Eng. Comput.*, vol. 39, no. 6, pp. 649–655, 2001.

[4] J. S. Paul, M. R. Reddy, and V. J. Kumar, "A transform domain SVD filter for suppression of muscle noise artefacts in exercise ECG's," *IEEE Trans. Biomed. Eng.*, vol. 47, no. 5, pp. 654–663, May 2000.

[5] N. V. Thakor and Y. S. Zhu, "Applications of adaptive filtering to ECG analysis: Noise cancellation and arrhythmia detection," *IEEE Trans. Biomed. Eng.*, vol. 38, no. 8, pp. 785–794, Aug. 1991.

[6] B. Acar and H. Koymen, "SVD based on line exercise ECG signal orthogonalization," *IEEE Trans. Biomed. Eng.*, vol. 46, no. 3, pp. 311–321, Mar. 1999.

[7] P. P. Kanjilal, S. Palit, and G. Saha, "Fetal ECG extraction from single-channel maternal ECG using singular value decomposition," *IEEE Trans. Biomed. Eng.*, vol. 44, no. 1, pp. 51–59, Jan. 1997.

[8] M. Richter, T. Schreiber, and D. T. Kaplan, "Fetal ECG extraction with nonlinear state-space projections," *IEEE Trans. Biomed. Eng.*, vol. 45, no. 1, pp. 133–137, Jn. 1998.

[9] P. C. Hansen, "Regularization tools: A matlab package for analysis and solution of discrete ill-posed problems," *Numerical Algorithms*, vol. 6, no. 1–2, pp. 1–35, 1994.

[10] P. E. McSharry, G. D. Clifford, L. Tarassenko, and L. A. Smith, "A dynamical model for generating synthetic electrocardiogram signals," *IEEE Trans. Biomed. Eng.*, vol. 50, no. 3, pp. 289–294, Mar. 2003.

[11] S. Iravanian and L. Tung, "A novel algorithm for cardiac biosignal filtering based on filtered residue method," *IEEE Trans. Biomed. Eng.*, vol. 49, no. 11, pp. 1310–1317, Nov. 2002.

[12] S. v. Huffel and P. Lemmerling, *Total Least Squares and Errors-in-Variables Modeling: Analysis, Algorithms and Applications*. Dordrecht, The Netherlands: Kluwer Academic, 2002.

[13] L. R. Rabiner and B. H. Juang, *Fundamentals of Speech Recognition*, ser. Signal Processing. Englewood Cliffs, NJ: PTR Prentice-Hall, 1993.

[14] G. W. Stewart, "Perturbation theory for the singular value decomposition," in *SVD and Signal Processing, II. Algorithms, Analysis and Applications*, R. J. Vaccaro, Ed. Amsterdam, The Netherlands: Elsevier, 1991, pp. 99–109.

[15] X. Hu and V. Nenov, "Multivariate ar modeling of electromyography for the classification of upper arm movements," *Clin. Neurophysiol.*, vol. 115, no. 6, pp. 1276–1287, 2004.

[16] A. L. Goldberger, L. A. N. Amaral, L. Glass, J. M. Hausdorff, P. C. Ivanov, R. G. Mark, J. E. Mietus, G. B. Moody, C.-K. Peng, and H. E. Stanley, "Physiobank, physiotoolkit, and physionet: Components of a new research resource for complex physiologic signals," *Circulation*, vol. 101, no. 23, pp. 215e–220e, 2000.

A High-Yield Fabrication Process for Silicon Neural Probes

Seung Jae Oh, Jong Keun Song, Jin Won Kim, and Sung June Kim*

***Abstract*—There is a great need for silicon microelectrodes that can simultaneously monitor the activity of many neurons in the brain. However, one of the existing processes for fabricating silicon microelectrodes—reactive-ion etching in combination with anisotropic KOH etching—breaks down at the wet-etching step for device release. Here we describe a modified wet-etching sidewall-protection technique for the high-yield fabrication of well-defined silicon probe structures, using a Teflon® shield and low-pressure chemical vapor deposition (LPCVD) silicon nitride. In the proposed method, a micro-tab holds each individual probe to the central scaffold, allowing uniform anisotropic KOH etching. Using this approach, we obtained a well-defined probe structure without device loss during the wet-etching process. This simple method yielded more accurate fabrication and an improved mechanical profile.**

***Index Terms*—High-yield process, neural prosthesis, sidewall protection, silicon neural probe, wet etching.**

I. INTRODUCTION

Silicon neural-probe technology has become one of the most important emerging technologies in BioMEMS applications since Wise *et al.* first described a photoengraved silicon probe [1]. A number of neural-probe technologies have been reported for use as advanced neural interfaces in neural prostheses [2]–[6]. These biomedical microdevices offer great promise for treating neurological disease and providing methods for the long-term study of the central [7]–[10] and peripheral [11], [12] nervous systems. We have previously reported

Manuscript received February 10, 2004; revised May 22, 2005. This work was supported in part by the Korean Science and Foundation (KOSEF) through the Nano-Bioelectronics and Systems Research Center, Seoul National University. *Asterisk indicates corresponding author.*

S. J. Oh, J. K. Song, and J. W. Kim are with the Nano Bioelectronics and Systems Research Center, Seoul National University, Seoul, 151-742, Korea.

*S. J. Kim is with the Nano Bioelectronics and Systems Research Center, ISRC Bldg. #104, Seoul National University, San 56-1, Sillim-dong, Kwanak-gu, Seoul, 151-742, Korea (e-mail: kimsj@snu.ac.kr).

Digital Object Identifier 10.1109/TBME.2005.862568

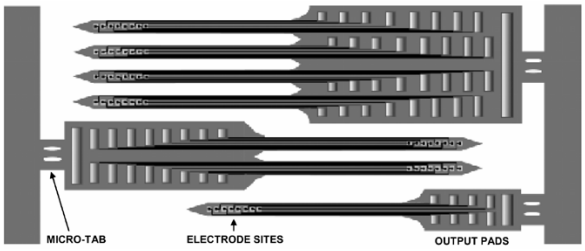

Fig. 1. A schematic drawing of probes containing one, two, and four shanks, where each shank has eight electrode sites. A micro-tab holds each individual probe to the central scaffold.

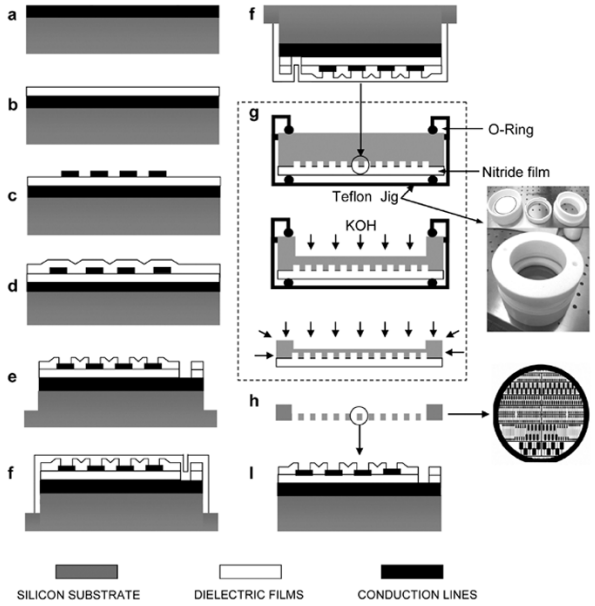

Fig. 2. Cross-sectional diagrams of the fabrication procedure using dry- and wet-etching techniques. The box (g) shows flow diagrams of the wet-etching process using Teflon® sealed to protect one side of the silicon wafer from KOH etchant. Silicon substrate is gray, doped poly-Si used as the conduction line and site is black, and dielectric layers are white.

on the development of a silicon neural probe fabricated by a silicon-etching process combining reactive-ion etching and anisotropic KOH etching in order to control the shank thickness [2], [13], [14]. This process was simple and inexpensive, but the product yield was limited by the wet-etching step used to release the devices from the silicon wafer. This paper describes a more effective design and fabrication process for silicon neural probes.

II. Material and Methods

The neural probe was designed so that each device was attached to a central scaffold by a narrow "break-off" micro-tab, as shown schematically in Fig. 1. This micro-tab is used to hold individual probes to the central scaffold so as to allow uniform KOH etching.

Fig. 2 shows a cross-sectional schematic view of the process flow for the neural probe. In the first step, polycrystalline silicon (poly-Si) used as an internal ground layer was deposited on a $\langle 100 \rangle$ -oriented, p-type double-polished silicon wafer using a low-pressure chemical vapor deposition (LPCVD) system, at 625 $^{\circ}\mathrm{C}$ and 300 mTorr, to a thickness of 3500 Å. This layer was then doped with $\mathrm{POCl_3}$ to a concentration of $10^{21}\ \mathrm{cm}^{-3}$ in a furnace at 950 $^{\circ}\mathrm{C}$ [Fig. 2(a)]. Triple dielectric layers ($\mathrm{SiO_2}$, 1000 Å; $\mathrm{Si_3N_4}$, 2000 Å; $\mathrm{SiO_2}$; 5000 Å) were deposited sequentially on the doped poly-Si layer [Fig. 2(b)]. The same type of doped poly-Si layer as described above was then deposited on the dielectric

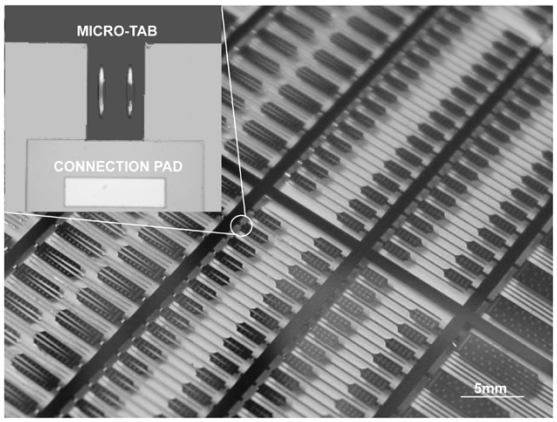

Fig. 3. Projection light micrograph of fabricated silicon probes. The boxed image shows the micro-tab used to hold individual probes to the central scaffold on the wafer.

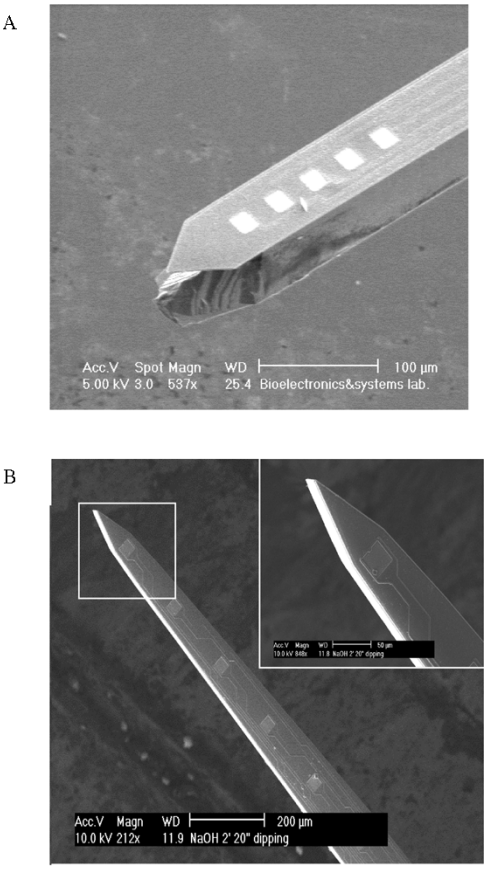

Fig. 4. (a) SEM views of a probe tip fabricated without the sidewall-protection technique for anisotropic KOH etching. (b) Well-defined probe structure fabricated using the sidewall-protection technique with LPCVD silicon nitride deposition.

layer, and patterned for recording sites and interconnections [Fig. 2(c)]. A second set of triple dielectric layers with the same structure was then deposited on top, to be used as insulating layers [Fig. 2(d)]. A photoresist mask was coated and patterned to permit deep reactive-ion silicon etching.

The deep-silicon etching was performed using the Bosch process, to a depth of 50 $\mu\mathrm{m}$ [Fig. 2(e)]. This etch depth determines the final shank thickness of the devices. To protect the sidewall of the shaft from anisotropic KOH etchant, LPCVD silicon nitride film was deposited

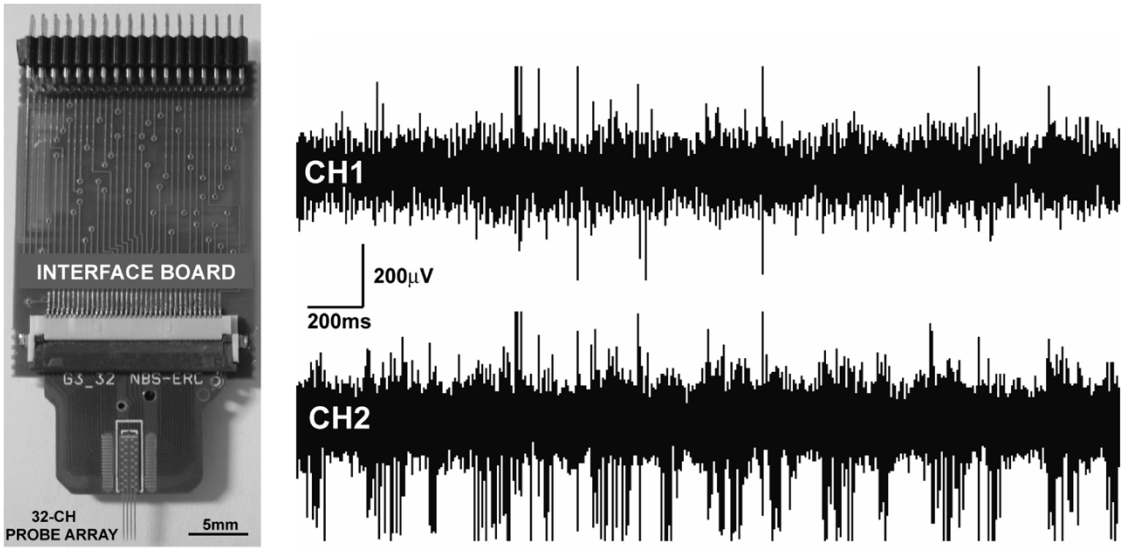

Fig. 5. (a) A photograph of the 32-channel, four-shank neural probe bonded to a printed circuit board for connection with external recording systems. (b) Action potentials recorded from the somatosensory cortex of an anesthetized rat, which are shown to be independent between adjoining channels.

[Fig. 2(f)] onto the patterned side. A Teflon® shield was used to protect one side from the KOH etching [Fig. 2(g)] [15].

The Teflon® shield was kept away from the protected side by mechanically pressing the side of the substrate to be protected onto an O-ring set into the main Teflon® piece. A second Teflon® piece screwed onto the main piece provides mechanical pressure along the periphery of the wafer, and it has an O-ring that matches the outer O-ring on the main piece. This Teflon® shield containing the wafer was immersed in a 30%wt KOH solution at 65 $^{\circ}\mathrm{C}$. The silicon on the backside of the wafer was etched until the structure was released [Fig. 2(h)]. The Teflon® shield was peeled off and then the LPCVD nitride film was removed by reactive-ion etching after the wet-etching step [Fig. 2(i)].

The electrophysiological performance of the silicon neural probe was verified by performing acute neural recording experiments. The craniotomy techniques are detailed elsewhere [16], [17]. All animals used for neural recording were treated in accordance with the animal research guidelines of Seoul National University. Sprague-Dawley rats (250 g, $n = 5$) were anesthetized with urethane (1 g/kg, i.p.) and then mounted on a stereotaxic frame. The silicon neural probe was driven into the target region of the brain using a precision manipulator. A multichannel acquisition system (Plexon Inc., Dallas, TX) was used for extracellular neural recording *in vivo*. The signals were amplified 10 000–30 000 times, bandpass filtered at 150 Hz to 5 kHz, and stored and analyzed on a personal computer.

III. Results and Discussion

We developed a process for the high-yield fabrication of a well-defined probe structure using a sidewall-protection technique. A total of 442 neural probes were obtained from a single 100-mm wafer; the shank of each probe was 5-mm or 10-mm long and 50 $\mu\mathrm{m}\times$ 128 $\mu\mathrm{m}$ in cross-section. Each probe has eight recording sites with an edge-to-edge spacing of 150 $\mu\mathrm{m}$ and 250 $\mu\mathrm{m}$, respectively. Fig. 3 shows a whole wafer containing these probe structures at a high density.

A beam structure with a well-defined depth is required for a neural probe in order to minimize tissue damage during probe insertion. This can be achieved using wet etching, either by time and etch-rate control or by etch-stop techniques. Etch stopping using boron doping is a powerful technique [18], [19], but creating a shaft thicker than 15 $\mu\mathrm{m}$ is difficult because of limits in the doping depth. We, therefore, used ion-reactive etching and anisotropic KOH etching for bulk silicon micromachining. The inability to use any compensation structures in the mask design with high-density structures makes it necessary to use different processing steps for the formation of sharp corners without any undercut [20]. Anisotropic etching of the probe tip using $\langle 100\rangle$-oriented silicon without sidewall protection is shown in Fig. 4(a), in which underetching of the probe sidewall is evident. This problem was solved by employing a sidewall-protection technique using LPCVD silicon nitride. This film is a suitable mask for anisotropic silicon etchant, and provides reliable long-term etch protection. In addition to the sidewall-protection technique, one-side KOH etching using a Teflon® shield was used while the other side was exposed to the etchant. Using these methods, we obtained a well-defined probe structure without device loss during the wet-etching process, as shown in Fig. 4(b). The probe tip was tapered to a few microns, allowing easy penetration into the neural tissue. There is minimal tissue response along the sides of shafts that are well sharpened and have a sufficiently small tip angle [21].

Fig. 5(a) shows a 32-channel, four-shank silicon neural probe bonded to a printed circuit board for connection with external recording systems. The recording properties of the neural probe can be determined *in vivo* by recording the unit neural activity and the amplitude-versus-depth distribution of the evoked potentials [13], [17]. An extracellular action potential recorded from the somatosensory cortex using a fabricated neural probe is shown in Fig. 5(b).

The extracellular potential contains spike waveforms from several units with an amplitude above the noise level. The action potentials being recorded at the different sites are clearly from independent adjoining channels.

IV. Conclusion

This paper has presented a micro-tab design and sidewall-protection method for anisotropic etching of silicon using LPCVD nitride film and a Teflon® shield. This technique allows the high-yield fabrication of a well-defined silicon neural probe without any undercutting. Neural probes fabricated by this process showed favorable performance in *in vivo* acute neural recording. These silicon-based electrode techniques represent an advanced technology for obtaining a high-performance neural interface.

REFERENCES

[1] K. D. Wise, J. B. Angell, and A. Starr, "An integrated circuitapproach to extracellular microelectrodes," *IEEE Trans. Biomed. Eng.*, vol. BME-17, pp. 238–247, 1970.

[2] S. J. Oh, J. K. Song, and S. J. Kim, "Neural interface with a silicon neural probe in the advanced of microtechnology," *Biotech. Bioprocess. Eng.*, vol. 8, no. 4, pp. 252–256, 2003.

[3] M. A. Nicolelis, "Brain-machine interfaces to restore motor function and probe neural circuits," *Nat. Rev. Neurosci.*, vol. 4, no. 5, pp. 417–422, 2003.

[4] J. K. Niparko, R. A. Altschuler, X. L. Xue, J. A. Wiler, and D. J. Anderson, "Surgical implantation and biocompatibility of central nervous system auditory prostheses," *Ann. Otol. Rhinol. Laryngol.*, pt. 1, vol. 98, no. 12, pp. 965–970, 1989.

[5] T. Hillman, A. N. Badi, R. A. Normann, T. Kertesz, and C. Shelton, "Cochlear nerve stimulation with a 3-dimensional penetrating electrode array," *Otol. Neurotol.*, vol. 24, no. 5, pp. 764–768, 2003.

[6] R. A. Normann, E. M. Maynard, P. J. Rousche, and D. J. Warren, "A neural interface for a cortical vision prosthesis," *Vis. Res.*, vol. 39, no. 15, pp. 2577–2587, 1999.

[7] J. Csicsvari, D. A. Henze, B. Jamieson, K. D. Harris, A. Sirota, P. Bartho, K. D. Wise, and G. Buzsaki, "Massively parallel recording of unit and local field potentials with silicon-based electrodes," *J. Neurophysiol.*, vol. 90, no. 2, pp. 1314–1323, 2003.

[8] J. D. Weiland and D. J. Anderson, "Chronic neuralstimulation with thin-film, iridium oxide electrode," *IEEE Trans. Biomed. Eng.*, vol. 47, no. 7, pp. 911–918, Jul 2000.

[9] P. J. Rousche and R. A. Normann, "Chronic recording capability of Utah intracortical electrode array in cat sensory cortex," *J. Neurosci. Meth.*, vol. 82, pp. 1–15, 1998.

[10] S. C. Bledsoe, S. E. Shore, and M. J. Guitton, "Spatial representation of corticofugal input in the inferiorcolliculus: A multicontact silicon probe approach," *Exp. Brain Res.*, vol. 153, no. 4, pp. 530–542, 2003.

[11] C. Gonzalez and M. Rodriguez, "A flexible perforated microelectrode array probe for action potential recording in nerve and muscle tissues," *J. Neurosci. Meth.*, vol. 72, no. 2, pp. 189–195, 1997.

[12] A. Branner and R. A. Normann, "A multielectrode array for intrafascicular recording and stimulation in sciatic nerve of cats," *Brain Res. Bull.*, vol. 51, no. 4, pp. 293–306, 2000.

[13] T. H. Yoon, E. J. Hwang, D. Y. Shin, S. I. Park, S. J. Oh, S. C. Jung, H. C. Shin, and S. J. Kim, "A micromachined silicon depth probe for multichannel neural recording," *IEEE Trans, Biomed. Eng.*, vol. 47, no. 8, pp. 1082–1087, Aug. 2000.

[14] S. J. Oh, J. K. Song, S. K. An, and S. J. Kim, "Properties of the doped polycrystalline silicon as site material for the micromachined silicon neural probe," *J. Mater. Sci. Lett.*, vol. 22, no. 2, pp. 131–3, 2003.

[15] J. T. Kung, A. N. Karnanicolas, and H. Lee, "A compact, inexpensive apparatus for one-side etching in KOH and HF," *Sensors Actuators A*, vol. 29, pp. 209–215, 1991.

[16] H. C. Shin, H. J. Park, and K. Chapin, "Differential phasic modulation of short and long latency afferent sensory transmission to single neurons in the primary somatosensory cortex in behaving rats," *Neurosci. Res.*, vol. 9, pp. 419–425, 1994.

[17] A. Bragin, J. F. Hetke, C. L. Wilson, D. J. Anderson, J. Engel Jr, and G. Buzsaki, "Multiple site silicon-based probesfor chronic recordings in freely moving rats:Implantation, recording and histological verification," *J. Neurosci. Meth.*, vol. 98, no. 1, pp. 77–82, 2000.

[18] D. J. Anderson, K. Najafi, S. J. Tanghe, D. A. Evans, K. L. Levy, J. F. Hetke, X. L. Xue, J. J. Zappia, and K. D. Wise, "Batch-fabricated thin-film electrodes for stimulation of the central auditory system," *IEEE Trans. Biomed. Eng.*, vol. 36, no. 7, pp. 693–704, Jul. 1989.

[19] B. Qui, K. D. Wise, and D. J. Anderson, "A high-yield microassembly structure for three-dimensional microelectrode arrays," *IEEE Trans. Biomed. Eng.*, vol. 47, no. 3, pp. 281–289, Mar. 2000.

[20] M. Giousouf, F. Assmus, and H. Kuck, "Structuring of convex corners using a reoxidation process-application to a tuing fork resonator made from (110)-silicon," *Sensors Actuators A*, vol. 76, pp. 416–24, 1999.

[21] D. J. Edell, V. V. Toi, V. M. McNeil, and L. D. Clark, "Factors influencing the biocompatibility of insertable silicon microshafts in cerebral cortex," *IEEE Trans. Biomed. Eng.*, vol. 39, no. 6, pp. 635–643, Jun. 1992.

The Effect of Interference Source Proximity on Cuff Imbalance

Iasonas F. Triantis and Andreas Demosthenous*

***Abstract*—The presence of cuff imbalance degrades the signal-to-interference (ENG/EMG) ratio in tripolar nerve cuff electrode recordings. Known causes of cuff imbalance include inhomogeneous tissue growth after cuff implantation and cuff manufacturing tolerances. In this paper, we report on an additional contribution to cuff imbalance that stems from variations in orientation and distance of the tripolar cuff relative to the external interference source. The latter is represented here by a dipole. Interference amplitude is also shown to depend on orientation and distance variations, here both factors included in the term "proximity." The study was conducted using field simulations and saline-bath experiments.**

***Index Terms*—Cuff imbalance, proximity effects, tripolar nerve cuffs.**

I. INTRODUCTION

Electroneurogram (ENG) recording techniques benefit from the use of tripolar cuffs because they assist in reducing interference from sources outside the cuff, such as electromyogram (EMG) generated from muscles nearby. To a first order of approximation, the nerve-tissue impedance is resistive; thus, the EMG potential inside the cuff varies *linearly* with distance along the cuff length [1]. This property is exploited by differential ENG amplifiers of the type described in [2]–[4] to provide interference cancellation. However, it has been widely reported that EMG contaminates ENG measurements [1]–[6], even when tripolar cuffs are used. This suggests that the cuff departs from ideal behavior, which results in what we shall term *cuff imbalance*. With reference to Fig. 1, cuff imbalance ($X_{\rm imb}$) is defined as

$$X_{\rm imb} = \left\{ \frac{|V_{AB}| - |V_{CB}|}{|V_{AB}| + |V_{CB}|} \right\} \times 100\% \tag{1}$$

where V_{AB} and V_{CB} are the voltages across electrode points AB and CB, respectively, caused by the external interference ionic current ($I_{\rm INT}$) flowing through the tissue resistances Z_{t1} and Z_{t2}. These voltages are anti-phase, but for $X_{\rm imb}$ to be zero, the condition $|V_{AB}| = |V_{CB}|$ must hold. If however $|V_{AB}| \neq |V_{CB}|$, then the presence of cuff imbalance will degrade ENG recordings. It should be noted that the degree of interference breakthrough will depend on the particular ENG amplifier used [2]–[4].

The major cause of cuff imbalance is inhomogeneous tissue re-growth after implantation [2]. An additional cause is cuff asymmetry due to imperfect electrode placement, but this can almost be eliminated with novel cuff fabrication techniques [7]. The effect of tissue re-growth is not possible to control but fortunately it is a very slow varying error [2]. In the study by Rahal *et al.* [5], cuff end-effects were reported to cause *nonlinearity* near the cuff ends. As a follow-up from that work, in this brief we show that these end-effects relate to the *proximity* of the external interference source to the cuff. Hence, cuff imbalance is also caused by cuff end-effects which depend

Manuscript received December 30, 2004; revised April 26. This work was supported in part by the United Kingdom Engineering and Physical Sciences Research Council (EPSRC) under Grant GR/S93790. *Asterisk indicates corresponding author.*

I. F. Triantis is with the Institute of Biomedical Engineering, Imperial College London, South Kensington Campus, London SW7 2AZ, U.K. (e-mail: i.tritanis@ic.ac.uk)

*A. Demosthenous is with the Department of Electronic and Electrical Engineering, University College London, Torrington Place, London WC1E 7JE, U.K. (e-mail: a.demosthenous@ee.ucl.ac.uk).

Digital Object Identifier 10.1109/TBME.2005.862569